ARTICLE

Check for updates

Journal of
Sensor Science and Technology

The Korean Sensors Society

Multi-Mode Sensor for Hydrogen Detection via Colorimetric and Electrical Signals Based on WO_3-Pd Films

Gwanggyo Jung[1], Jiyoun Lee[1], Minwook Kang[1], Haechan Jang[1], Somin Kim[1], and Hyungtak Seo[1,2,+]

[1] *Department of Energy Systems Research 206, Ajou University, World cup-ro, Yeongtong-gu, Suwon-si, Gyeonggi-do, Republic of Korea*
[2] *Department of Materials Science and Engineering, 206, Ajou University, World cup-ro, Yeongtong-gu, Suwon-si, Gyeonggi-do, Republic of Korea*

Cite This: *J. Sens. Sci. Technol. Vol. 34, No. 6 (2025) 601-609*

https://doi.org/10.46670/JSST.2025.34.6.601

ABSTRACT: Hydrogen is an eco-friendly energy source widely used in various industries, but its high flammability and explosion risk require rapid and accurate detection. This study optimized a WO_3-Pd-based multi-mode hydrogen detection sensor, integrating electrical and optical signals for high-sensitivity monitoring. WO_3 exhibits chemochromic properties, changing color upon hydrogen exposure, whereas Pd acts as a catalytic layer, facilitating hydrogen dissociation and diffusion. Using RF-magnetron sputtering and E-beam deposition, the thickness of WO_3 and Pd was precisely controlled to achieve optimal sensing performance. The sensor successfully detected hydrogen concentrations from 1% to 10% and at the ppm level, with electrical signal responses and colorimetric changes occurring within 5 s. Additionally, a color difference (ΔE^*) of 53.64 and a transmittance change (ΔT) of 34% confirmed clear visual detection. Finally, a sensor module with real-time monitoring and alarm functions was implemented, demonstrating its practicality as a reliable hydrogen detection technology. The results of this study is expected to contribute to enhancing the stability and safety of future hydrogen-based energy systems.

KEYWORDS: *Hydrogen gas sensors, Oxide-based sensor, WO_3, Pd*

1. INTRODUCTION

Hydrogen is an eco-friendly energy carrier with a high gravimetric energy density and is widely utilized in various industrial sectors such as fuel-cell vehicles, industrial processes, and hydrogen refueling stations [1]. With recent global emphasis on carbon neutrality, hydrogen energy has emerged as a key alternative to conventional fossil fuels. However, because hydrogen is lighter than air, it diffuses rapidly into the atmosphere, and its colorless and odorless nature makes detecting leaks difficult [2]. In addition, because hydrogen has a wide flammability range, even a small leak can easily lead to severe accidents, making rapid and accurate detection technologies essential.

Currently, various sensor technologies for hydrogen detection are being actively investigated, including semiconductor oxide, catalytic, electrochemical, and resistive-type sensors. Among these, semiconductor oxide sensors have attracted significant interest owing to their high sensitivity and fast response. In particular, tungsten trioxide (WO_3) has emerged as a promising sensing material because it exhibits both electrical and optical variations upon exposure to hydrogen [3].

WO_3 exhibits colorimetric properties, in which its electrical conductivity increases and its color changes upon interaction with hydrogen. This phenomenon enables simultaneous visual detection and quantitative analysis of hydrogen [4].

However, conventional single-mode sensors are highly susceptible to various environmental factors, such as temperature, humidity, and impurity concentration, which can degrade their performance and limit their long-term stability [5]. Although colorimetric detection provides an intuitive visual response, achieving quantitative accuracy is difficult, whereas resistance-based detection is easily affected by ambient conditions, which leads to reliability issues [6]. Therefore, multi-mode sensors are required to overcome the limitations of conventional sensors and achieve more reliable hydrogen detection.

A multi-mode sensor that utilizes both electrical and optical sensors enhances the overall reliability of the sensor and provides more accurate information on hydrogen concentration

[+]Corresponding author: hseo@ajou.ac.kr
Received : Sep. 15, 2025, Revised : Sep. 26, 2025, Accepted : Oct. 11, 2025

changes [7]. In particular, under real operating conditions, such as industrial environments, various external factors can influence sensor responses, highlighting the importance of multi-mode sensors even more essential.

In this study, a WO_3-Pd-based multi-mode hydrogen sensor was developed to maximize sensing performance through an optimized structural design. WO_3 exhibits distinct color variations when exposed to hydrogen, whereas palladium serves as a catalytic layer that dissociates hydrogen molecules and facilitates their diffusion. The thicknesses of the WO_3 and Pd layers were optimized to investigate the effect of their combination on the hydrogen-sensing performance, enabling the establishment of an optimized multi-mode sensor configuration. This paper proposes a novel hydrogen sensing system based on multi-mode sensing, presenting a pathway toward a highly precise and reliable hydrogen monitoring technology for future applications.

2. EXPERIMENTAL

2.1 Sensor fabrication

2.1.1 Sensor structure

The multi-mode hydrogen-sensing sensor was fabricated by sequentially depositing WO_3 and Pd thin films on a glass substrate, followed by the formation of electrodes and subsequent dicing into individual sensor chips. The entire sensor structure consisted of four layers sequentially stacked from the bottom as follows: Glass substrate / WO_3 sensing layer / Pd catalytic layer / Cr-Au electrode layer.

A transparent glass substrate was used to ensure optical transmittance for colorimetric sensing. A WO_3 thin film was deposited on the glass substrate using an RF magnetron sputtering system, which served as the primary sensing layer. Subsequently, a Pd catalytic layer was deposited on top of the WO_3 film via e-beam evaporation. The Pd layer promoted hydrogen molecule dissociation and hydrogen ion diffusion into the WO_3 matrix, thereby improving the response characteristics of the sensor.

2.1.2 WO_3 deposition

The WO_3 thin film was deposited using an RF magnetron sputtering system (Sci & Tech, Korea, 13.56 MHz) with a high-purity WO_3 target (VTM, Korea). A glass substrate (Sigma Aldrich, USA) was used for all the samples, and the deposition process was conducted under fixed parameters, with the WO_3 thickness set as the only variable.

The sputtering process was performed under identical conditions for all samples: a working pressure of 10 mTorr, an Ar flow rate of 30 sccm, and an RF power of 150 W. The film thickness was controlled by adjusting the deposition time, and the effect of the WO_3 thickness variation was systematically analyzed.

To maintain consistent hydrogen dissociation conditions, we fixed the Pd layer thickness at 4 nm for all the samples. This configuration was designed to precisely evaluate the influence of the WO_3 film thickness on the hydrogen interaction and the overall sensing performance.

2.1.3 Pd deposition

Pd, which serves as a catalytic layer that dissociates hydrogen molecules into ionic forms, was deposited on top of the WO_3 thin film using an e-beam evaporator (Sci & Tech, Korea) with a high-purity Pd target (99.995% purity, VTM, Korea). The deposition process was performed under a pressure of 3 μTorr with a deposition rate of 0.1 nm/s. To investigate the effect of the Pd layer thickness on the sensing characteristics, we varied the Pd layer thickness to 2, 4, 6, and 8 nm.

The transmittance change (ΔT) and surface roughness (RMS) were measured for each sample to evaluate the influence of the deposition conditions of the Pd catalytic layer on the optical and physical properties of the WO_3 film. For experimental consistency, the WO_3 layer was fixed at a sputtering time of 70 min (corresponding to sample 4 in Table 1).

To analyze the electrical response characteristics quantitatively, we deposited an additional metal electrode on top of the Pd catalytic layer. Electrode deposition was performed using an e-beam evaporator (Sci & Tech, Republic of Korea) using high-purity Cr (99.995% purity, VTM, Korea) and Au (99.999% purity, VTM, Korea).

A Cr layer was deposited as an adhesion layer, and an Au layer with a thickness of 3 nm was subsequently deposited to ensure electrical conductivity with a thickness of 50 nm. The electrodes were fabricated with an active area of 1 mm × 1 mm corresponding to each sensing region, enabling the stable and accurate measurement of resistance variations during hydrogen exposure.

2.2 Sensor package design

After the deposition, the multilayer structure was diced into individual sensor chips, each forming a single sensing unit. The

Table 1. Deposition time of WO_3.

Sample Number	Sputter Time	Pd Thickness
1	10 min	4 nm
2	30 min	
3	50 min	
4	70 min	
5	90 min	

Table 2. Deposition thickness of Pd

Pd Thickness	WO_3 Sputter Time
2 nm	70 min
4 nm	
6 nm	
8 nm	

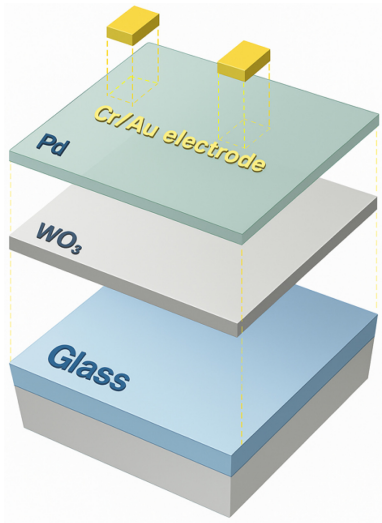

Fig. 1. 3D schematic structure image of WO_3-Pd sensor.

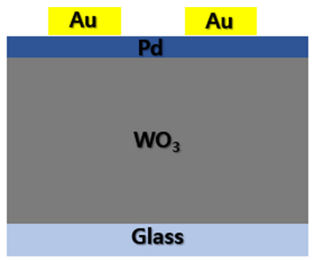

Fig. 2. Schematic cross-sectional image of WO_3-Pd Sensor.

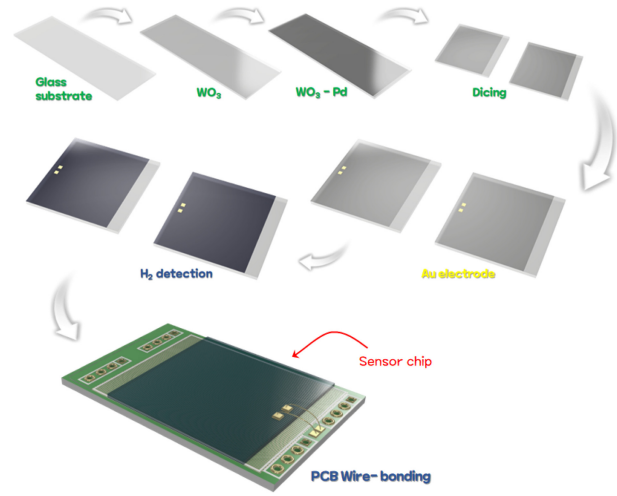

Fig. 3. WO_3-Pd hydrogen sensor chip fabrication up to PCB wire-bonding.

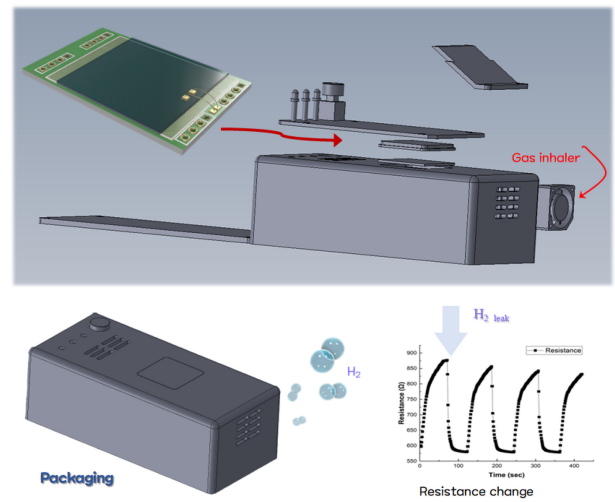

Fig. 4. Illustration of the sensor packaging process and resistance-based hydrogen detection in a sealed module.

fabricated sensor chips were then mounted onto a printed circuit board (PCB), and electrical connections between the sensor electrodes and the PCB circuitry were established through a wire bonding process. This process resulted in a packaged sensor module, enabling the electrical response of the sensor to be transmitted to external measurement equipment.

Based on the fabricated hydrogen sensing chip, a modular multi-mode hydrogen-sensing system was designed and developed considering practical operating environments. This system was not limited to a sensing function but was also equipped with additional features to enhance real-time responses and user convenience.

To effectively capture hydrogen gas and improve sensing sensitivity, we installed a miniature gas intake unit on the upper part of the module. This intake unit directs the gas flow into the sensor chamber, and its internal structure was optimized through a flow-path design to ensure that hydrogen is rapidly and selectively delivered to the sensing region. Consequently, the system achieved a shorter response time and enabled rapid detection, even at trace hydrogen concentrations.

In addition, when the detected hydrogen concentration exceeds a predefined threshold, the system automatically identifies the conditions and provides immediate warning signals to the user. The alarm module integrates both visual LED blinking and auditory buzzer alerts, which are activated according to pre-set criteria through automatic data analysis of the sensor output. These multi-alert functions enable intuitive and rapid confirmation of hydrogen leakage in industrial or enclosed environments, ensuring both the safety and practical applicability of the developed system.

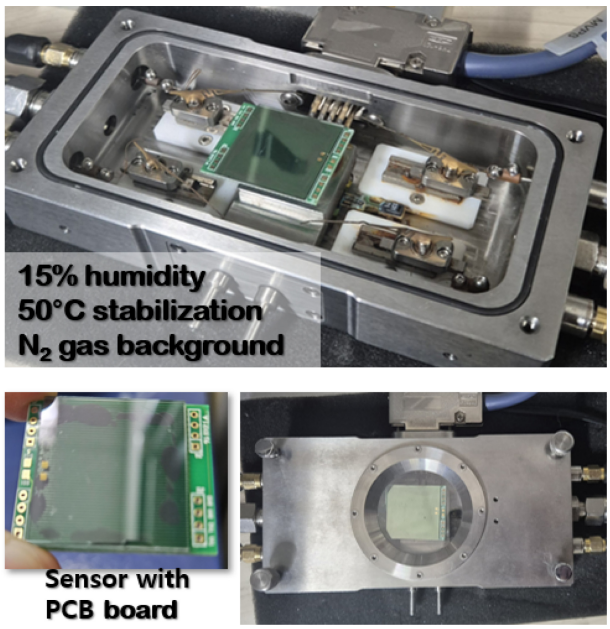

Fig. 5. Electrical signal measurement using MFC and I-V probe station.

2.3 Electrical signal measurement

To evaluate the electrical performance of the fabricated WO_3-Pd-based hydrogen sensor, we employed a mass flow controller (MFC, Atovac, Korea), a sensor probe station (Nextron, Korea), and an I–V source meter (Keithley 2400, USA). This measurement setup enables precise control of the gas flow rate and environmental conditions, such as temperature and humidity, making it suitable for quantitative analysis under simulated operating environments. Measurements were conducted under stabilized conditions of relative humidity (RH) 15% and 50°C, with N_2 used as the background gas to control the hydrogen concentration. The sensor chip was mounted inside the probe station and its electrical response before and after hydrogen exposure was monitored in real time. Hydrogen gas was precisely introduced according to the set flow rate, and the change in the resistance of the sensor was used as a key indicator of the hydrogen-sensing behavior. From these data, major sensing parameters such as response, response time, and recovery time were quantitatively evaluated.

2.4 Colorimetric signal measurement

Ultraviolet–visible (UV–Vis) spectroscopy was used to evaluate the colorimetric characteristics of the fabricated sensors. This analysis enables the quantitative assessment of the optical changes in the sensor, and the color difference (ΔE*) value was introduced to quantify the degree of color variation. The ΔE* was calculated using the following equation:.

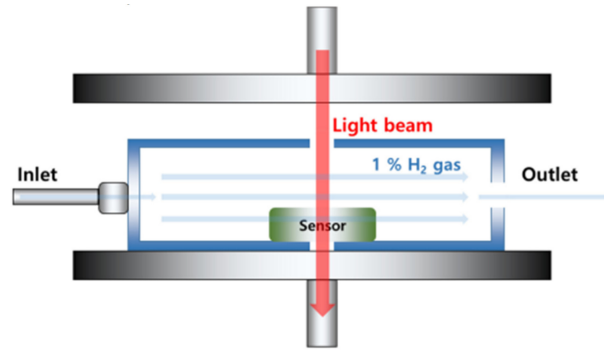

Fig. 6. Schematic of UV–Vis equipment for colorimetric detection.

$$\Delta E^* = \sqrt{(L_2 - L_2)^2 + (a_2 - a_1)^2 + (b_2 - b_1)^2} \quad (1)$$

3. RESULTS AND DISCUSSION

3.1 Variation in sensing characteristics with WO_3 thickness

Fig. 7 shows the variation in WO_3 film thickness as a function of deposition time, as determined by atomic force microscopy (AFM). As the deposition time increased, the WO_3 film thickness increased linearly, from 100.8 nm for Sample #1 (WO_3-10m) to 868.6 nm for Sample #5 (WO_3-90m), as summarized in Table 1.

The AFM analysis revealed that the RMS roughness increased from 1.642 to 3.346 nm with increasing film thickness, confirming that the surface roughness varied depending on the deposition conditions.

Fig. 9 presents the transmission electron microscopy–energy dispersive spectroscopy (TEM-EDS) cross-sectional image of the WO_3 film deposited by sputtering for 70 min. The analysis indicated that, during the initial deposition stage, a dense and compact film was formed, whereas when the thickness exceeded 150 nm, the morphology transitioned into a columnar and porous structure.

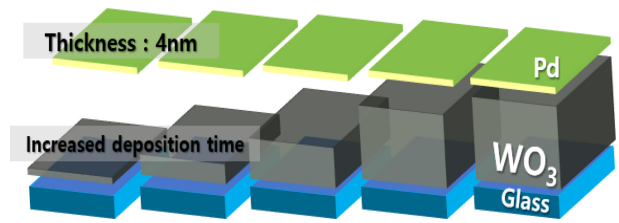

Fig. 7. Schematic illustration of WO_3 thickness increase with sputtering time.

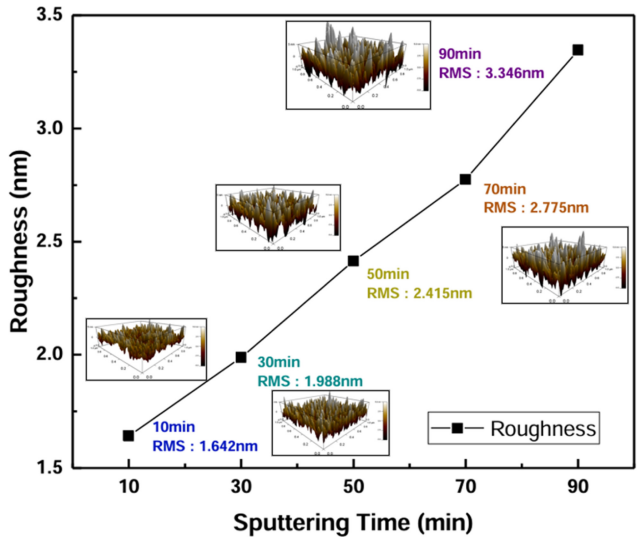

Fig. 8. Time-dependent changes in the surface roughness of WO_3.

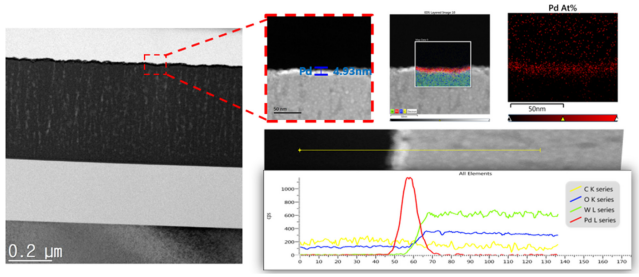

Fig. 9. Cross-sectional TEM image and corresponding EDS line-scan analysis of the Pd/WO_3 interface

Although the Pd catalytic layer was deposited under the same e-beam evaporation conditions, the measured Pd thickness varied depending on the WO_3 film thickness. For the thicker WO_3 layers, the Pd thickness was 4.93 nm, whereas that for the thinner WO_3 layers was approximately 3.97 nm. This difference suggests that the variation in surface roughness affected the uniformity of Pd deposition, leading to a dispersed distribution of Pd particles rather than a continuous film. In particular, the Pd nanoparticles tended to remain well-dispersed rather than agglomerate on surfaces with higher roughness.

Furthermore, as the thickness of the WO_3 film increased, the surface roughness gradually increased. Such morphological variations induced scattering and non-uniform distribution of Pd particles, thereby affecting the deposition characteristics. Consequently, we confirmed that the surface morphology of WO_3 had a critical influence on the growth behavior and microstructural formation of the Pd layer.

Fig. 10 shows the correlation between the surface roughness and electrical response characteristics of WO_3 thin films with

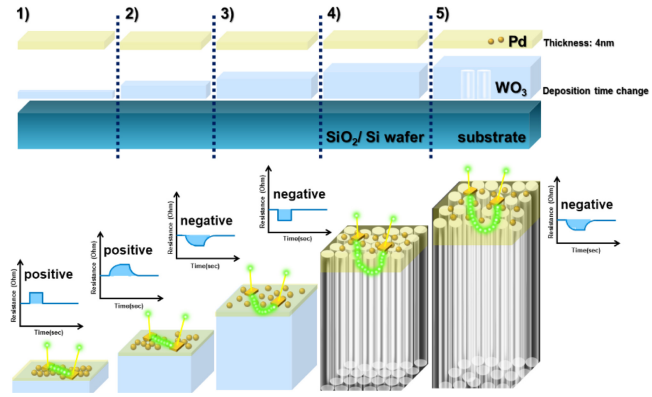

Fig. 10. Effect of WO_3 thickness on electrical signal behavior.

varying thicknesses. A comparison between Sample #4 (WO_3–70 m) and Sample #1 (WO_3–10 m) revealed distinct differences in the microstructural features and corresponding electrical responses resulting from changes in the film thickness.

For Sample #4, the WO_3 film with a thickness of approximately 800 nm exhibited a dense morphology within the initial 200 nm region, followed by a transition to a columnar porous structure as the deposition proceeded. This morphological transition facilitated the penetration of hydrogen atoms (H), thereby promoting the formation of conductive pathways within the WO_3 matrix. The measured surface roughness of this sample was 2.775 nm, indicating that the deposited Pd nanoparticles were distributed non-uniformly and in a scattered form. Thus, hydrogen atoms dissociated by the Pd catalyst combined with oxygen species within the WO_3 matrix to form hydroxyl (OH) groups, leading to a reduction of WO_3 to WO_{3-x}. This reduction process increased the number of free W 5d electrons, thereby enhancing electrical conductivity and resulting in a negative resistance change.

In contrast, Sample #1, which consisted of a 100 nm-thick WO_3 film, maintained a compact morphology throughout the entire layer. The surface roughness was relatively low (1.642 nm), and the Pd particles formed a continuous interconnected structure. In this configuration, hydrogen adsorbed on the Pd surface formed PdH_x, which interrupted the electron flow within the metallic layer, causing a positive resistance change.

Overall, as the WO_3 film thickness increases, changes in surface roughness and microstructure directly affect Pd deposition and the electrical response during hydrogen sensing. Therefore, controlling the WO_3 microstructure and optimizing the Pd nanoparticle distribution are critical factors for enhancing sensing performance and achieving optimal sensor design.

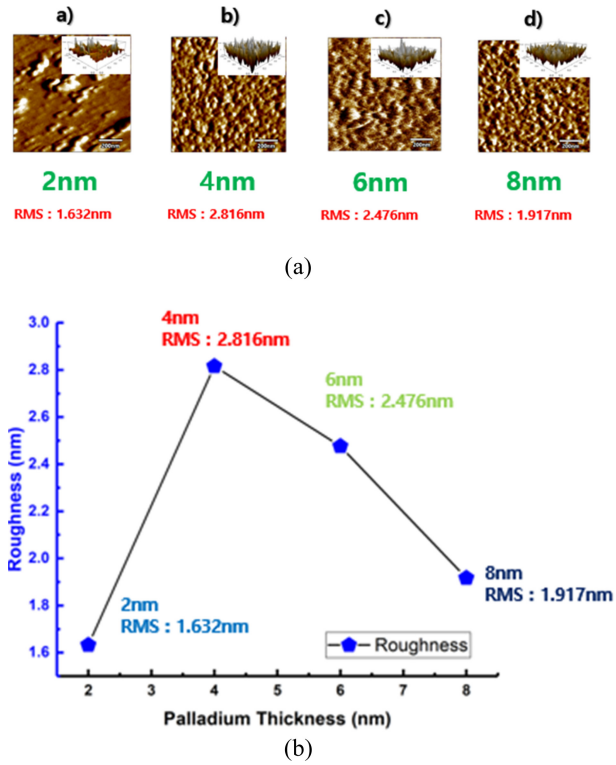

Fig. 11. AFM Surface morphology and corresponding RMS roughness variation of Pd films with different thicknesses. (a) Surface roughness differences observed using AFM at varying Pd thicknesses. (b) Surface morphology of Pd films with varying thickness

3.2 Optimization of transmittance by adjusting Pd thickness

Fig. 11 shows the surface roughness characteristics of the Pd films with varying thicknesses, as analyzed using AFM. When the Pd thickness increased from 2 to 8 nm, clear differences in the surface morphology and roughness were observed.

a) At a thickness of 2 nm, the surface roughness was 1.632 nm, indicating a uniform and smooth surface and suggesting that the Pd nanoparticles were evenly distributed during the initial deposition stage.

b) When the thickness increased to 4 nm, the surface roughness increased to 2.816 nm, and the surface exhibited a highly non-uniform morphology, which can be attributed to the growth and agglomeration of Pd particles during the deposition process.

c) At 6 nm, the surface roughness decreased slightly to 2.476 nm and the particle boundaries became more ordered, implying that localized coalescence among the Pd particles had begun.

d) At 8 nm, the roughness further decreased to 1.917 nm, indicating a densely packed surface structure, which suggests that enhanced coalescence among the Pd particles resulted in a locally ordered surface morphology.

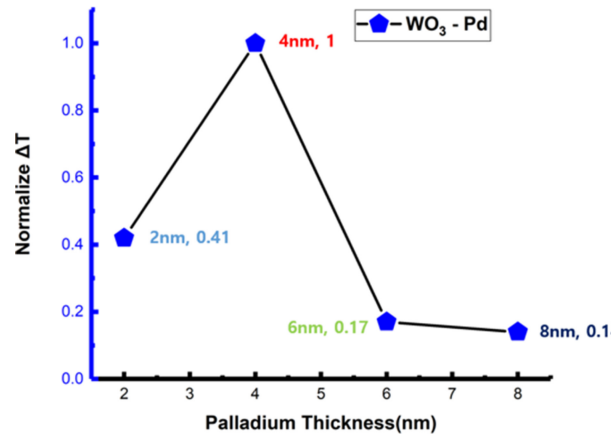

Fig. 12. Normalized optical transmittance as a function of Pd thickness.

This trend indicates that the roughness of the Pd film varied nonlinearly with thickness, initially increasing owing to particle growth and then decreasing as the film became denser.

Larger surface roughness resulted in a greater exposed surface area of Pd, thereby enhancing its reactivity with hydrogen and influencing the amount of hydrogen diffusing into the WO_3 layer. From this perspective, the 4 nm-thick Pd film provided the most favorable structure for hydrogen dissociation and interaction between Pd and WO_3.

Fig. 12 shows the ΔT values of Pd films with different thicknesses. The ΔT values were normalized with respect to the highest response observed at a Pd thickness of 4 nm.

When the Pd thickness was 2 nm, the normalized ΔT value was 0.41 owing to the limited reactive surface area of the thin film. In contrast, at 4 nm, the ΔT reached its maximum, indicating that the active surface area of Pd was maximized, resulting in highly efficient hydrogen dissociation and adsorption. However, when the Pd thickness increased to 6 and 8 nm, the ΔT values decreased sharply to 0.17 and 0.14, respectively. This degradation can be explained by particle agglomeration and a reduced effective reaction area, which hinder hydrogen diffusion and deteriorate the sensing performance. In particular, excessive Pd thickness reduces the optical transmittance of the Pd layer itself, suppressing the colorimetric variation originating from the underlying WO_3.

Therefore, the 4-nm Pd film exhibited the highest surface roughness and strongest transmittance response, confirming that it provides the optimal thickness for hydrogen sensing. These results emphasize the importance of precisely controlling the Pd deposition thickness to enhance sensor sensitivity.

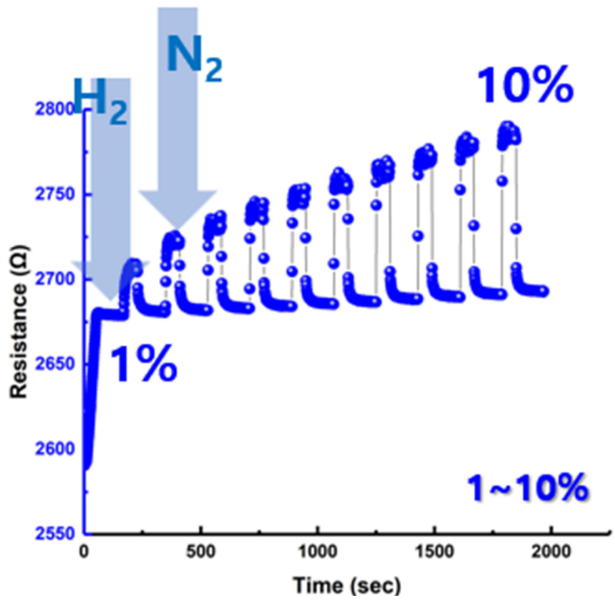

Fig. 13. Response to hydrogen exposure in the range of 1%–10%.

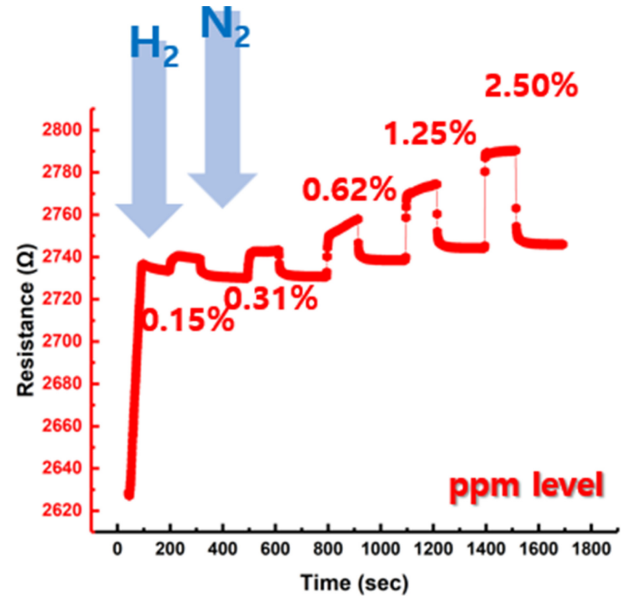

Fig. 14. Response to hydrogen exposure in the range of ppm levels.

3.3 Electrical signal measurement results

The WO_3-Pd hydrogen sensor was exposed stepwise to hydrogen concentrations ranging from 1% to 10%, followed by nitrogen purging to remove residual gas, while monitoring the time-dependent variation in electrical resistance.

The concentration sensitivity and recovery characteristics of the sensor were quantitatively evaluated using this process. Upon the introduction of hydrogen, the sensor exhibited an increase in resistance, which originated from the metal–hydride phase transition occurring in the Pd layer. When hydrogen molecules dissociate and are adsorbed onto the Pd surface, they diffuse into the lattice, causing a transition from the pure metallic phase (α-Pd) to a low-hydrogen solid solution phase (α-PdH_x). As the hydrogen concentration increases, this further transforms into the β-PdH_x phase. During this phase transition, the Pd lattice expands by approximately 3%–4%, reducing the mean free path of electrons and increasing the scattering rate, thereby leading to an overall increase in electrical resistance.

Conversely, when the hydrogen flow is stopped and nitrogen is introduced, the hydrogen atoms trapped within the Pd lattice desorb, resulting in the decomposition of the PdH_x phase and the restoration of the metallic α-Pd phase. As this process proceeds, the conduction pathway recovers and the sensor resistance gradually returns to its initial state.

Repeated hydrogen–nitrogen cycling tests demonstrated that the sensor exhibited consistent resistance changes with excellent reversibility and stability. Notably, as the hydrogen concentration increased from 1% to 10%, the proportion of the β-PdHx phase formation increased correspondingly, leading to a progressive rise in resistance variation. This result confirms that the fabricated sensor exhibits a quantitative and concentration-dependent response to hydrogen.

To further investigate the low-concentration response, we introduced hydrogen stepwise from 0.15% to 2.50% (ppm), and the resistance variation over time was measured.

Upon hydrogen exposure, the resistance increased, and then decreased again upon nitrogen purging, confirming a typical reversible behavior that demonstrates stable sensor operation. As shown in Fig. 14, the resistance increased incrementally with increasing hydrogen concentration, indicating that the surface reaction on WO_3 proceeds proportionally to hydrogen concentration even at ppm levels. In particular, under 0.15% hydrogen exposure, the resistance changed from 2720 to 2740 Ω, confirming that the sensor can detect very low hydrogen concentrations sensitively. As the hydrogen concentration increased to 0.31% and 0.62%, the resistance variation became more pronounced, showing a clear and consistent electrical response even for small differences in the hydrogen concentration.

At relatively higher hydrogen concentrations of 1.25% and 2.50%, the resistance further increased to 2760 Ω, exhibiting a nearly linear correlation between resistance change and hydrogen concentration.

Consequently, the fabricated sensor maintained a high sensitivity even at ppm hydrogen concentrations, exhibiting concentration-dependent and quantitative response characteristics, thereby demonstrating its potential as a reliable hydrogen-sensing device.

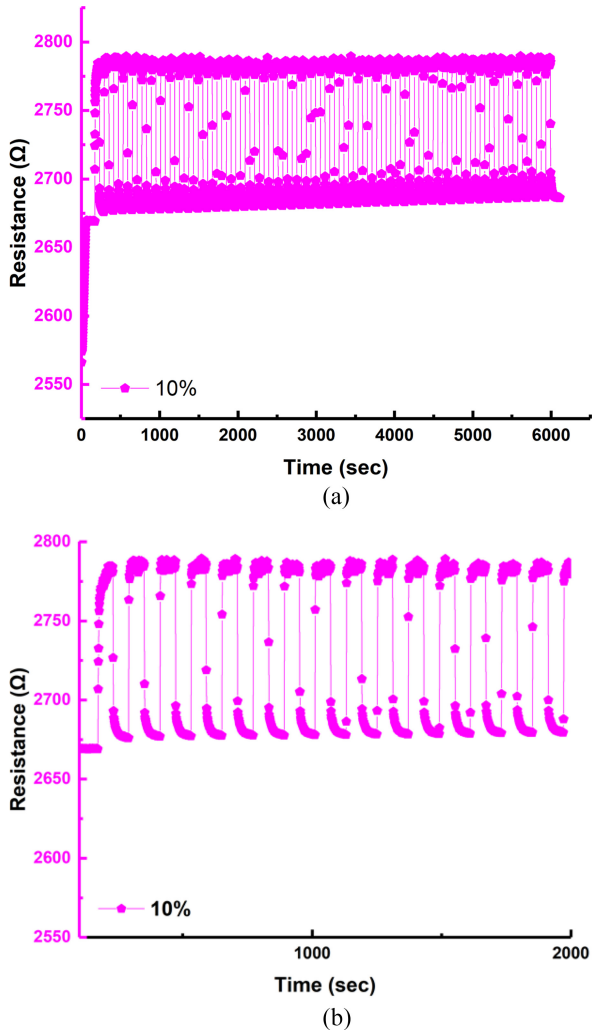

Fig. 15. Electrical stability and repeatability characteristics of the WO3-Pd hydrogen sensor. (a) Electrical response of the sensor under 50 repeated exposures to 4% hydrogen (b) Enlarged view of repeated resistance increase in a specific section.

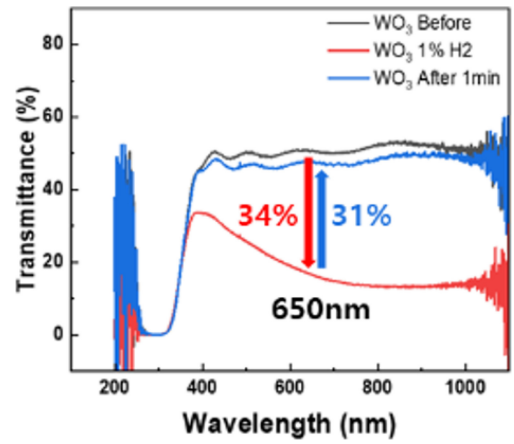

Fig. 16. Transmittance response to 1% hydrogen exposure

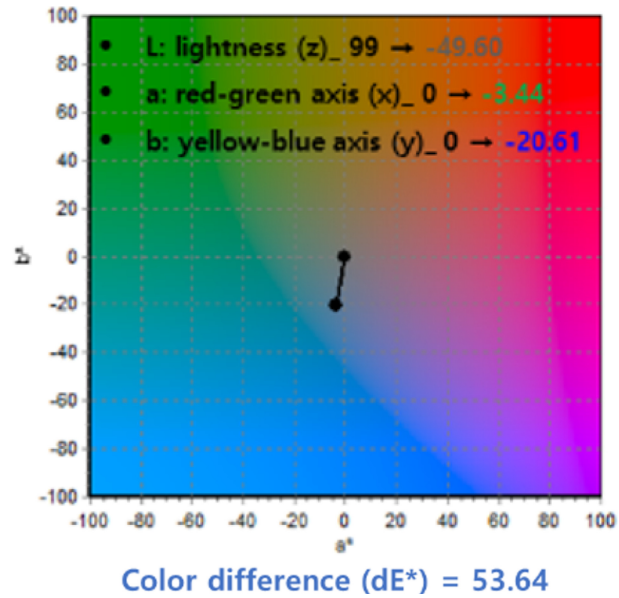

Fig. 17. Change in sensor color difference upon hydrogen exposure

Fig. 15 shows the experimental results of the fabricated sensor under repeated hydrogen exposure. Repeatability and reliability were evaluated over 50 consecutive exposure-purge cycles using 4% hydrogen gas. Through all 50 cycles, the resistance variation pattern remained highly consistent, demonstrating excellent repeatability and reversible hydrogen characteristics. During each hydrogen exposure and removal phase, the resistance values were clearly distinguishable, showing stable and reproducible changes within the same range across all cycles. Moreover, the sensor exhibited negligible variations in sensitivity, response time, and recovery time, even after repeated hydrogen exposure. These results confirm that the sensor maintains a reliable and stable sensing performance, ensuring long-term operational durability for practical hydrogen monitoring applications.

3.4 Colorimetric signal measurement results

Fig. 16 shows the quantitative analysis of the transmittance variation for the WO_3-Pd-based hydrogen sensor upon exposure to 1% hydrogen gas, as measured using UV–Vis spectroscopy. The sensor exhibited a sharp decrease in transmittance when exposed to hydrogen, followed by clear reversible colorimetric recovery once the gas was purged. In particular, at a wavelength of 650 nm, the transmittance decreased by 34% immediately after hydrogen exposure and recovered by 31% after gas removal, demonstrating the excellent optical response of the sensor.

The measured ΔE* calculated using Equation (1) in the CIE Lab color space was 53.64, which corresponds to a distinct color change readily distinguishable by the naked eye. This

result indicates that the colorimetric response of the sensor upon hydrogen exposure was visually pronounced, demonstrating its practical potential as a color-based hydrogen detection system.

4. CONCLUSION

In this study, a WO_3-Pd-based multi-mode hydrogen sensor capable of simultaneous electrical and optical detection was designed, and its performance was quantitatively evaluated through structural optimization and response analysis. The sensor was constructed by combining the colorimetric property of WO_3 with the catalytic hydrogen dissociation capability of Pd, and the thicknesses of both layers were optimized to maximize sensitivity, response time, and recovery characteristics. In the electrical sensing mode, the sensor exhibited a distinct resistance variation proportional to the hydrogen concentration. Upon exposure to 1% hydrogen gas, a rapid response time of less than 5 s with excellent reversibility was observed. The sensing range was extended from 0.15% to 10%, and reproducible resistance changes were consistently observed, even in the low-concentration region. The optical sensing mode was based on the colorimetric response of the WO_3 film, quantitatively analyzed using UV–Vis spectroscopy and color difference evaluation. At a wavelength of 650 nm, the ΔT decreased by 34% upon hydrogen exposure and recovered by 31% after gas removal. The calculated ΔE^* was 53.64, indicating a clearly perceptible color change easily distinguishable by the naked eye, thereby confirming the feasibility of visual hydrogen detection. Based on these characteristics, the sensor system was implemented in a module designed for practical applications. The module incorporates a gas-intake structure, an automated alarm system that is activated when the hydrogen concentration exceeds a preset threshold, and LED indicators that respond to concentration changes, enabling intuitive monitoring of the sensor status by the user. Consequently, the developed sensor demonstrated excellent response and reproducibility for both electrical and optical signals, providing an effective technological foundation for the advancement and commercialization of real-time hydrogen detection systems.

CRediT Authorship Contribution Statement

Gwanggyo Jung: Investigation, Data curation, Investigation, Writing - original draft. **Jiyoun Lee:** Investigation, Data curation. **Minwook Kang:** Data curation. **Haechan Jang:** Investigation. **Somin Kim:** Investigation. **Hyungtak Seo:** Supervision, Writing – review and editing, Funding acquisition, Resources.

Declaration of Competing Interest

The authors declare that they have no competing financial interests or personal relationships that may have influenced the work reported in this paper.

Acknowledgement

This work was supported by the Korea Energy Technology Evaluation and Planning (Project No: (RS-2024-00457128) funded by the Ministry of Trade, Industry and Energy, Republic of Korea.

REFERENCES

[1] F. Yang, T. Wang, X. Deng, J. Dang, Z. Huang, S. Hu, et al., Review on hydrogen safety issues: Incident statistics, hydrogen diffusion, and detonation process, Int. J. Hydrogen Energy 46 (2021) 31467–31488.
[2] H. Li, X. Cao, Y. Liu, Y. Shao, Z. Nan, L. Teng, et al., Safety of hydrogen storage and transportation: An overview on mechanisms, techniques, and challenges, Energy Rep. 8 (2022) 6258–6269.
[3] A. Nikfarjam, S. Fardindoost, A.I. Zad, Fabrication of Pd Doped WO3 Nanofiber as Hydrogen Sensor, Polymers 5(2013) 45–55.
[4] S. Kim, B. Maeng, Y. Yang, K. Kim, D. Jung, Hybrid Hydrogen Sensor Based on Pd/WO_3 Showing Simultaneous Chemiresistive and Gasochromic Response, Nanomaterials 13 (2023) 2563.
[5] G. Korotcenkov, Metal oxides for solid-state gas sensors: What determines our choice?, Mater. Sci. Eng. B 139 (2007) 1–23.
[6] A. Mirzaei, J.H. Kim, H.W. Kim, S.S. Kim, Gasochromic WO3 Nanostructures for the Detection of Hydrogen Gas: An Overview, Appl. Sci. 9 (2019) 1775.
[7] Z. Park, Y.H. Cho, Y.S. Shim, Gasochromic Hydrogen Sensors based on Pd-functionalized WO_3 film: A Brief Review, J. Sens. Sci. Technol. 34 (2025) 231–239.